Chapter 5

Nonlinear Dynamics and Control of Aerial Robots

Mahmut Reyhanoglu and Muhammad Rehan

Additional information is available at the end of the chapter

http://dx.doi.org/10.5772/intechopen.69641

Abstract

Aerial robotics is one of the fastest growing industry and has a number of evolving applications. Higher agility make aerial robots ideal candidate for applications like rescue missions especially in difficult to access areas. This chapter first derives the complete nonlinear dynamics of an aerial robot consisting of a quadcopter with a two-link robot manipulator. Precise control of such an aerial robot is a challenging task due to the fact that the translational and rotational dynamics of the quadcopter are strongly coupled with the dynamics of the manipulator. We extend our previous results on the control of quadrotor UAVs to the control of aerial robots. In particular, we design a backstepping and Lyapunov-based nonlinear feedback control law that achieves point-to-point control of the areal robot. The effectiveness of this feedback control law is illustrated through a simulation example.

Keywords: quadcopter, robot manipulator, backstepping method, nonlinear control

1. Introduction

The recent surge of interest in applications involving unmanned aerial vehicles (UAVs) has inspired several research efforts in UAV dynamic modeling and control. In particular, nonlinear control of fixed-wing UAVs has attracted considerable research efforts during recent years both for civilian and military purposes. The control approaches developed for fixed-wing UAVs include gain scheduling, model predictive control, backstepping, sliding mode, nested saturation, fuzzy control, H_∞ control, dynamic inversion based control, model reference adaptive control, and model based fault tolerant control [1–12].

While control applications involving fixed-wing UAVs have been widely investigated in recent literature, quadrotor UAV (quadcopter) control applications are growing in popularity due to their maneuverability and versatility. Quadcopters offer practical advantages over fixed-wing

UAVs in military and civilian applications involving search and rescue, area mapping, and surveillance. However, actuator constraints, sensor limitations, and the high degree of nonlinearity and uncertainty inherent in the system dynamics present specific challenges in control system design for quadcopters. Linear control approaches, such as PID, LQR or LQG are popularly utilized to address the quadcopter control problem [13–15]. Although linear control methods have been shown to perform well in their respective quadcopter control tasks, the effectiveness of linear control methods can only be guaranteed over a limited range of operating conditions. The highly agile nature of quadcopters necessitates the development of control methods that can be applied over a wide range of time-varying, uncertain, and potentially adversarial operating conditions. To achieve reliable quadcopter control over a wider operational envelope, several nonlinear control methods have recently been presented. Popular nonlinear control methods for quadrotor systems include backstepping, feedback linearization, dynamic inversion, adaptive control, Lyapunov-based robust control, fuzzy-model approach, and sliding mode control [16–19]. In Ref. [16], a passivity-based quaternion feedback control strategy is presented for a hover system (quadrotor UAV test bed), which achieves asymptotic attitude regulation. The proposed control design incorporates the input voltage constraints inherent in practical UAV systems. A rigorous Lyapunov-based analysis is provided to prove asymptotic regulation of the hover system attitude to a desired set point. In Ref. [17], a sliding mode control (SMC) strategy is presented for a quadrotor-based hover system, which achieves asymptotic attitude regulation in the presence of electrical and physical constraints. A sliding mode observer is employed to estimate the angular velocities. In addition, the proposed control design incorporates the input voltage constraints inherent in practical systems. A rigorous Lyapunov-based analysis is provided to prove asymptotic regulation of the hover system attitude to a desired set point.

Aerial robotics is one of the fastest growing industry and has a number of evolving applications. Higher agility make aerial robots ideal candidate for applications like rescue missions especially in difficult to access areas. Furthermore, swarm robotics (multiple robot working together) is another exciting application of the aerial robotics, for example coordinated assembly at higher altitudes. These robots can behave like individuals working in a group without centralized control. Researchers have developed intelligent control algorithms for the swarms after deep study of animal behavior in herds, bird flocks and fish schools. In some applications, for an aerial robot, linear control theory works well but these control techniques are effective in a limited operating regions. Moreover, the motion of arm induces disturbances to the quadcopter dynamics so the linear controllers lose their effectiveness during operation and sometime the closed loop system becomes unstable. In order to accomplish complex missions in presence of uncertainties in the environment, to achieve better maneuverability and precise 3D position and attitude control, nonlinear control techniques have been found effective [20–27], In Ref. [20] a set of nonlinear control laws have been proposed for aerial manipulator that provide asymptotic attitude and position tracking. Backstepping-based nonlinear control scheme for automatic trajectory tracking for aerial manipulators has been proposed in Refs. [22, 24].

In this chapter, we extend our results on the control of quadcopters to the control of aerial robots. We derive the complete nonlinear dynamics of an aerial robot consisting of a quadcopter with a two-link robot manipulator. Precise control of such a robot is a challenging task because attitude and position dynamics of the quadcopter are strongly coupled with the

dynamics of the manipulator. We develop nonlinear control laws that ensure the control of position and attitude of the aerial robot. Simulation results are included to demonstrate the effectiveness of the control laws.

2. Mathematical model

This section formulates the dynamics of an aerial robot consisting of a quadcopter with a two-link robot manipulator. The quadcopter is represented as a base body and the links as internal bodies. The equations of motion are expressed in terms of the three dimensional translational velocity vector, the attitude, the angular velocity, and the internal (shape) coordinates representing the configuration of the two links.

2.1. Multibody vehicle dynamics

Following the development in [28], let $v \in \mathbb{R}^3$, $\omega \in \mathbb{R}^3$, and $\eta \in \mathbb{S}^1 \times \mathbb{S}^1$ denote the base body translational velocity vector, the base body angular velocity vector, and the vector of internal coordinates, respectively. In these variables, the kinetic energy has the form $T = T(v, \omega, \eta, \dot{\eta})$, which is $SE(3)$-invariant in the sense that it does not depend on the base body position and attitude. The equations of motion of the quadrotor with internal dynamics are shown to be given by:

$$\frac{d}{dt}\frac{\partial T}{\partial v} + \hat{\omega}\frac{\partial T}{\partial v} = F_t, \tag{1}$$

$$\frac{d}{dt}\frac{\partial T}{\partial \omega} + \hat{\omega}\frac{\partial T}{\partial \omega} + \hat{v}\frac{\partial T}{\partial v} = \tau_r, \tag{2}$$

$$\frac{d}{dt}\frac{\partial T}{\partial \dot{\eta}} - \frac{\partial T}{\partial \eta} = \tau_s, \tag{3}$$

where $F_t \in \mathbb{R}^3$, $\tau_r \in \mathbb{R}^3$ denote the vectors of generalized control forces and generalized control torques, respectively, that act on the base body, and $\tau_s \in \mathbb{R}^3$ is the vector of joint torques. For a given vector $a = [a_1\ a_2\ a_3]^T \in \mathbb{R}^3$, the skew-symmetric matrix $\hat{a}$ defines the corresponding cross-product operation $a\times$, given by

$$\hat{a} = \begin{bmatrix} 0 & -a_3 & a_2 \\ a_3 & 0 & -a_1 \\ -a_2 & a_1 & 0 \end{bmatrix}. \tag{4}$$

Note that Eqs. (1) and (2) are identical to Kirchhoff's equations [29], which can also be expressed in the form of Euler-Poincaré equations.

2.2. Nonlinear equations of motion

Consider an aerial robot that consists of a quadcopter with a two DOF manipulator arm moving in a three-dimensional space as shown in **Figure 1**, where $p = [x\ y\ z]^T$ denotes the

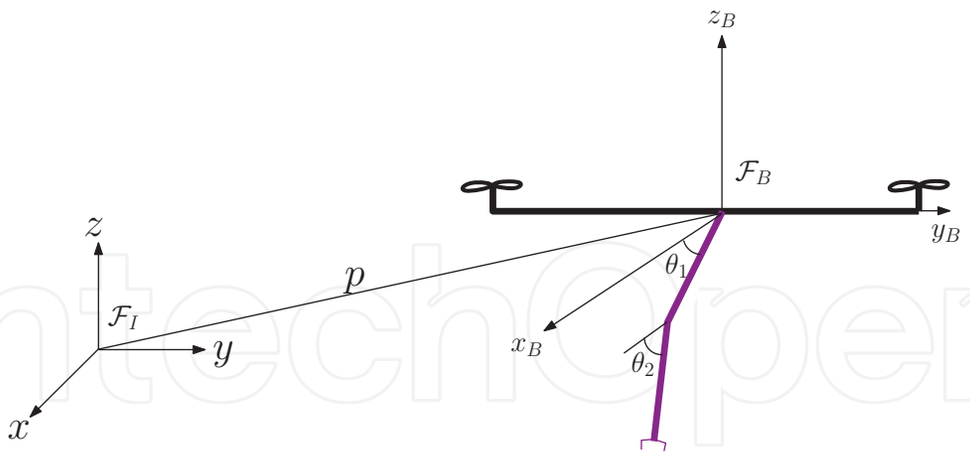

Figure 1. Model of a quadcopter with a robotic arm.

inertial position of the center of mass of the quadcopter. Denote by xyz axes the inertial frame $\mathcal{F}_1$ and by $x_B\ y_B\ z_B$ axes the body-fixed frame $\mathcal{F}_B$ with the origin at the CM of the quadcopter. Let R denote the attitude matrix of the quadcopter and $(v,\ \omega)$ be the translational and angular velocities of the CM of the quadrotor in $\mathcal{F}_B$. Then, the translational and rotational kinematics can be expressed as

$$\dot{p} = Rv, \tag{5}$$

$$\dot{R} = R\hat{\omega}. \tag{6}$$

The quadcopter consists of four propellers connected to a rigid frame. Each propeller is mounted on the frame at a distance l from the origin. The quadcopter has a mass m and inertia matrix J defined with respect to the axes of rotation. Due to symmetry of the system, J is diagonal, that is, $J = \text{diag}\{J_{xx},\ J_{yy},\ J_{zz}\}$. We refer to rotation about the x_B-axis as roll, rotation about the y_B-axis as pitch, and rotation about the z_B-axis as yaw. The propellers generate lift forces

$$F_i = b\Omega_i^2 = bK_v^2V_i^2, \tag{7}$$

where Ω_i, V_i denote, respectively, the angular rate and input voltage for propeller i, and b is the thrust coefficient. The total thrust is given by

$$F_p = \sum_{i=1}^{4} F_i e_3 = bK_v^2(V_1^2 + V_2^2 + V_3^2 + V_4^2)e_3, \tag{8}$$

where $e_3 = [0\ 0\ 1]^T \in \mathbb{R}^3$ is the third standard basis vector.

Note that, as shown in **Figure 2**, propellers 1 and 3 rotate clockwise, and propellers 2 and 4 rotate counter-clockwise. By balancing the torque between opposing propellers, the roll and pitch angle can be controlled. Since all four propellers generate a net torque about the yaw axis, the yaw angle can be controlled by balancing the torque generated by clockwise and counter-clockwise rotating propellers.

http://dx.doi.org/10.5772/intechopen.69641

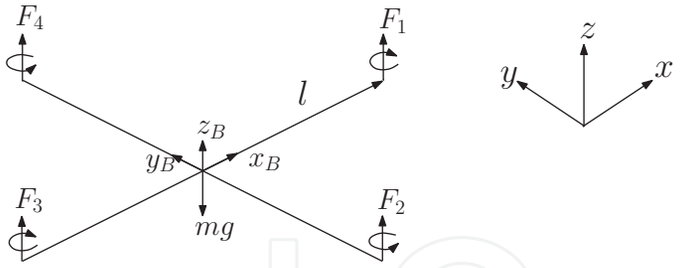

Figure 2. Model of the quadcopter.

The arm is attached at the CM of the quadcopter and it can only move in xz-plane of the body-fixed frame F_B. The physical constants are the quadcopter mass m, the link masses m_i, i = 1,2, and the payload mass m_p. Let l_{c_i} denote the distance from joint i to the CM of link i and l_i be the length of link i. The position vectors for the CM of the links and the payload with respect to the CM of the base body in F_B can be written as

$$\rho_1 = [\, l_{c_1} \cos\theta_1 \quad 0 \quad l_{c_1} \sin\theta_1 \,]^T, \tag{9}$$

$$\rho_2 = [\, l_1 \cos\theta_1 + l_{c_2} \cos\theta_2 \quad 0 \quad l_1 \sin\theta_1 + l_{c_2} \sin\theta_2 \,]^T, \tag{10}$$

$$\rho_p = [\, l_1 \cos\theta_1 + l_2 \cos\theta_2 \quad 0 \quad l_1 \sin\theta_1 + l_2 \sin\theta_2 \,]^T. \tag{11}$$

Let $F_t = F_g + F_p$, where F_g and F_p denote, respectively, the gravitational force acting on aerial robot and the total thrust generated by the four propellers. Also let $\tau_r = \tau_g + \tau_p$, where τ_g and τ_p are the torque acting on the aerial robot due to gravity and the torque generated by the propellers, respectively.

Clearly, F_g and τ_g can be computed as

$$F_g = -m_t g R^T e_3, \tag{12}$$

$$\tau_g = -g[m_1\rho_1 + m_2\rho_2 + m_p\rho_p] \times R^T e_3, \tag{13}$$

where $m_t = m + m_1 + m_2 + m_p$.

The generalized torque vector τ_p (expressed in the body frame) comprises the following components:

- Propellers 2 and 4 generate a moment $l(F_4 - F_2) = blK_v^2(V_4^2 - V_2^2)$ about the roll axis.
- Propellers 1 and 3 generate a moment $l(F_3 - F_1) = blK_v^2(V_3^2 - V_1^2)$ about the pitch axis.
- The sum of all torques about z-axis is $dK_v^2(V_1^2 - V_2^2 + V_3^2 - V_4^2)$ and causes a yaw moment.
- The rotation of the propellers causes the gyroscopic effect $J_r K_v \omega_y (V_1 - V_2 + V_3 - V_4)$ about the roll-axis and $-J_r K_v \omega_x (V_1 - V_2 + V_3 - V_4)$ about the pitch-axis.

Here d denotes the drag coefficient, l is the distance from the pivot to the motor, and J_r is the rotor inertia. Combined, the generalized torque τ_p can be expressed as

$$\tau_p = \begin{bmatrix} blK_v^2(V_4^2 - V_2^2) + J_r\omega_y\Omega_r \\ blK_v^2(V_3^2 - V_1^2) - J_r\omega_x\Omega_r \\ dK_v^2(V_1^2 - V_2^2 + V_3^2 - V_4^2) \end{bmatrix}, \tag{14}$$

where $\Omega_r := K_v(V_1 - V_2 + V_3 - V_4)$ is the overall residual angular speed of the propellers.

Let $\eta = [\theta_1 \ \theta_2]^T$ denote the shape variables. Then, the linear and angular velocities of each link, and the linear velocity of the payload can be expressed in $\mathcal{F}_B$ as

$$v_i = v + \hat{\omega}\rho_i + \frac{\partial \rho_i}{\partial \eta}\dot{\eta} = v - \hat{\rho}_i\omega + \frac{\partial \rho_i}{\partial \eta}\dot{\eta}, \ i = 1, 2, \tag{15}$$

$$\omega_i = \omega + \dot{\theta}_i e_2 = \omega + C_i(\eta)\dot{\eta}, \ i = 1, 2, \tag{16}$$

$$v_p = v + \hat{\omega}\rho_p + \frac{\partial \rho_p}{\partial \eta}\dot{\eta} = v - \hat{\rho}_p\omega + \frac{\partial \rho_p}{\partial \eta}\dot{\eta}, \tag{17}$$

where $e_2 = [0\ 1\ 0]^T \in \mathbb{R}^3$ is the second standard basis vector. The total kinetic energy can now be expressed as

$$T(v, \omega, \eta, \dot{\eta}) = \frac{1}{2}mv^Tv + \frac{1}{2}\omega^TJ\omega + \frac{1}{2}\sum_{i=1}^{2}(m_i{v_i}^Tv_i + {\omega_i}^TJ_i\omega_i) + \frac{1}{2}m_p{v_p}^2, \tag{18}$$

where $J_i = R_i^T\bar{J}_iR_i$ is the inertia matrix of the ith link with respect the body frame F_B, R_i is the rotation matrix of the ith link, which is given by

$$R_i = \begin{bmatrix} \cos\theta_i & 0 & \sin\theta_i \\ 0 & 1 & 0 \\ -\sin\theta_i & 0 & \cos\theta_i \end{bmatrix}, \quad i = 1, 2, \tag{19}$$

and $\bar{J}_i$ denotes the inertia matrix of the ith link with respect to $x_iy_iz_i$-axes attached to the link. Assuming the two links are made up of homogeneous rods, $\bar{J}_i$ can be expressed as

$$\bar{J}_i = \begin{bmatrix} 0 & 0 & 0 \\ 0 & \frac{1}{12}m_il_i^2 & 0 \\ 0 & 0 & \frac{1}{12}m_il_i^2 \end{bmatrix}. \tag{20}$$

Applying Kirchhoff's equations (1) and (2), the complete nonlinear equations of motion can be obtained as

http://dx.doi.org/10.5772/intechopen.69641

$$\begin{bmatrix} M & K & B_t \\ K^T & \bar{J} & B_r \\ B_t^T & B_r^T & \overline{m} \end{bmatrix} \begin{bmatrix} \dot{v} \\ \dot{w} \\ \ddot{\eta} \end{bmatrix} = \begin{bmatrix} F_t \\ \tau_r \\ \tau_s \end{bmatrix}$$
$$- \begin{bmatrix} \hat{w}M & \dot{K} + \hat{w}K & \dot{B}_t + \hat{w}B_t \\ \dot{K}^T + \hat{w}K^T + \hat{v}M & \dot{\bar{J}} + \hat{w}\bar{J} + \hat{v}K & \dot{B}_a + \hat{w}B_a + \hat{v}B_t \\ \dot{B}_t^T & \dot{B}_a^T & \dot{\overline{m}} \end{bmatrix} \begin{bmatrix} v \\ w \\ \dot{\eta} \end{bmatrix} + \begin{bmatrix} 0 \\ 0 \\ \frac{\partial L}{\partial \eta} \end{bmatrix}, \tag{21}$$

where

$$M = m_t I_{3\times 3}, \tag{22}$$

$$\bar{J} = J + m_1 \hat{\rho}_1^T \hat{\rho}_1 + m_2 \hat{\rho}_2^T \hat{\rho}_2 + m_p \hat{\rho}_p^T \hat{\rho}_p + J_1 + J_2, \tag{23}$$

$$\overline{m} = m_1 \frac{\partial \rho_1}{\partial \eta}^T \frac{\partial \rho_1}{\partial \eta} + m_2 \frac{\partial \rho_2}{\partial \eta}^T \frac{\partial \rho_2}{\partial \eta} + m_p \frac{\partial \rho_p}{\partial \eta}^T \frac{\partial \rho_p}{\partial \eta} + C_1^T J_1 C_1 + C_2^T J_2 C_2, \tag{24}$$

$$K = -m_1 \hat{\rho} 1 - m_2 \hat{\rho}_2 - m_p \hat{\rho}_p, \tag{25}$$

$$B_t = m_1 \frac{\partial \rho_1}{\partial \eta} + m_2 \frac{\partial \rho_2}{\partial \eta} + m_p \frac{\partial \rho_p}{\partial \eta}, \tag{26}$$

$$B_r = m_1 \hat{\rho}_1 \frac{\partial \rho_1}{\partial \eta} + m_2 \hat{\rho}_2 \frac{\partial \rho_2}{\partial \eta} + m_p \hat{\rho}_p \frac{\partial \rho_p}{\partial \eta} + J_1 C_1 + J_2 C_2. \tag{27}$$

Complete description of the above coefficient matrices are given in the appendix. The objective is to simultaneously control the 6 DOF motion of the quadcopter and the 2 DOF internal dynamics of the robot arm using only 4 propellers and 2 joint torque motors. In this regard, equations of motion given by (21) represents an interesting example of underactuated mechanical systems. In our previous research [30–32], we have developed theoretical controllability and stabilizability results for a large class of underactuated mechanical systems using tools from nonlinear control theory. We have also developed effective nonlinear control design methodologies [32] that we applied to several examples of underactuated mechanical systems, including underactuated space vehicles [33].

3. Nonlinear control design

The translational and rotational dynamics of the quadcopter are coupled with the dynamics of its robotic arm; this makes controller design very complicated. The equations of motion in component form are given by

$$M\dot{v} + K\dot{\omega} + B_t\ddot{\eta} = F_t - \hat{\omega}Mv - (\dot{K} + \hat{\omega}K)\omega - (\dot{B}_t + \hat{\omega}B_t)\dot{\eta}, \tag{28}$$

$$K^T\dot{v} + \bar{J}\dot{\omega} + B_a\ddot{\eta} = \tau_r - (\dot{K}^T + \hat{\omega}K^T + \hat{v}M)v - (\dot{\bar{J}} + \hat{\omega}\bar{J} + \hat{v}K)\omega - (\dot{B}_a + \hat{\omega}B_a + \hat{v}B_t)\dot{\eta}, \tag{29}$$

$$B_t^T \dot{v} + B_a^T \dot{\omega} + \overline{m}\ddot{\eta} = \tau_s - \dot{B}_t^T v - \dot{B}_a^T \omega - \dot{\overline{m}}\dot{\eta} + \frac{\partial L}{\partial \eta}. \tag{30}$$

Eq. (28) can be rewritten as

$$M\dot{v} = F_t - \hat{\omega} M v + F_d, \tag{31}$$

where

$$F_d = -K\dot{\omega} - B_t\ddot{\eta} - (\dot{K} + \hat{\omega}K)\omega - (\dot{B}_t + \hat{w}B_t)\dot{\eta}. \tag{32}$$

Eq. (31) can be simplified as

$$\begin{bmatrix} \ddot{x} \\ \ddot{y} \\ \ddot{z} \end{bmatrix} = \begin{bmatrix} 0 \\ 0 \\ -g \end{bmatrix} + R\hat{e}_3 u_1 + \overline{F}_d. \tag{33}$$

where $\overline{F}_d = F_d/m_t$ and

$$u_1 = bK_v^2(V_1^2 + V_2^2 + V_3^2 + V_4^2)/m_t, \tag{34}$$

Similarly, Eq. (29) can be rewritten as

$$\overline{J}\dot{\omega} = \tau_r - (\dot{\overline{J}} + \hat{\omega}\overline{J})\omega + \tau_d, \tag{35}$$

where

$$\tau_d = -K^T\dot{v} - B_a\ddot{\eta} - (\dot{K}^T + \hat{\omega}K^T + \hat{v}M)v - \hat{v}K\omega - (\dot{B}_a + \hat{\omega}B_a + \hat{v}B_t)\dot{\eta}. \tag{36}$$

Eq. (35) can be simplified as

$$\dot{\omega} = \overline{J}^{-1}\tau_r - \overline{J}^{-1}(\dot{\overline{J}} + \hat{\omega}\overline{J})\omega + \overline{\tau}_d, \tag{37}$$

where $\overline{\tau}_d = \overline{J}^{-1}\tau_d$.

Ignoring $\overline{F}_d$ and $\overline{\tau}_d$ in Eqs. (33) and (37), equations of motion can be expressed as

$$\ddot{x} = (\cos\phi \sin\theta \cos\Psi + \sin\phi \sin\Psi)u_1, \tag{38}$$

$$\ddot{y} = (\cos\phi \sin\theta \sin\Psi - \sin\phi \cos\Psi)u_1, \tag{39}$$

$$\ddot{z} = -g + (\cos\phi \cos\theta)u_1, \tag{40}$$

$$\begin{bmatrix} \dot{\omega}_x \\ \dot{\omega}_y \\ \dot{\omega}_z \end{bmatrix} = \overline{J}^{-1}\left(\tau_g + \begin{bmatrix} J_r\omega_y\Omega_r \\ -J_r\omega_x\Omega_r \\ 0 \end{bmatrix} - (\dot{\overline{J}} + \hat{\omega}\overline{J})\omega\right) + \begin{bmatrix} u_2 \\ u_3 \\ u_4 \end{bmatrix}, \tag{41}$$

http://dx.doi.org/10.5772/intechopen.69641

where

$$\begin{bmatrix} u_2 \\ u_3 \\ u_4 \end{bmatrix} = \bar{J}^{-1} \begin{bmatrix} blK_v^2(V_4^2 - V_2^2) \\ blK_v^2(V_3^2 - V_1^2) \\ blK_v^2(V_1^2 - V_2^2 + V_3^2 - V_4^2) \end{bmatrix}. \tag{42}$$

We now design a nonlinear controller based on integrator backstepping. If ϕ, θ and Ψ are small (sin $\theta \approx \theta$ and cos $\theta \approx \theta$), then $\omega \approx [\dot{\phi}\ \dot{\theta}\ \dot{\Psi}]^T$ and $\dot{\omega} \approx [\ddot{\phi}\ \ddot{\theta}\ \ddot{\Psi}]^T$, and hence the equation of motions can be simplified as

$$\ddot{x} = \theta u_1, \tag{43}$$

$$\ddot{y} = -\phi u_1, \tag{44}$$

$$\ddot{z} = -g + u_1, \tag{45}$$

$$\ddot{\phi} = f_1(\phi, \theta, \Psi) + u_2, \tag{46}$$

$$\ddot{\theta} = f_2(\phi, \theta, \Psi) + u_3, \tag{47}$$

$$\ddot{\Psi} = f_3(\phi, \theta, \Psi) + u_4, \tag{48}$$

where

$$\begin{bmatrix} f_1 \\ f_2 \\ f_3 \end{bmatrix} = \bar{J}^{-1} \left(\tau_g + \begin{bmatrix} J_r \dot{\theta} \Omega_r \\ -J_r \dot{\phi} \Omega_r \\ 0 \end{bmatrix} - (\dot{\bar{J}} + \hat{\omega} \bar{J}) \begin{bmatrix} \dot{\phi} \\ \dot{\theta} \\ \dot{\Psi} \end{bmatrix} \right). \tag{49}$$

3.1. Controller design

In this section a nonlinear controller is designed to stabilize the system (43)–(48) to the desired equilibrium configuration $(x, y, z, \phi, \theta, \Psi) = (x_d, y_d, z_d, \phi_d, \theta_d, \Psi_d)$.

We choose u_1 as

$$u_1 = g - |z - z_d|^a \, sign\,(z - z_d) - |\dot{z}|^b \, sign\,(\dot{z}), \tag{50}$$

where $b \in (0, 1)$, $a > b / (2 - b)$, $i = 1,2$, are controller parameters. The feedback law (50) controls the quadcopter z-dynamics to $(z, \dot{z}) = (z_d, 0)$ in finite time [34] so that $u_1 \to g$ in finite time.

After reaching the desired altitude, Eqs. (43) and (44) take the following form:

$$\ddot{x} = g\theta, \tag{51}$$

$$\ddot{y} = -g\phi. \tag{52}$$

We now apply a backstepping method to design the controls u_2 and u_3 to stabilize the system to the equilibrium at $(x, y, \phi, \theta) = (x_d, y_d, \phi_d, \theta_d)$.

Assume that θ and ϕ are virtual inputs for the x and y subsystems, respectively. Stabilizing feedback functions for the x-subsystem is given by

$$\theta = -k_1(x - x_d) - k_2\dot{x}, \tag{53}$$

$$\phi = k_3(y - y_d) + k_4\dot{y}, \tag{54}$$

where $k_i > 0$, $i = 1,\ldots,4$, so that

$$\ddot{x} + gk_2\dot{x} + gk_1(x - x_d) = 0, \tag{55}$$

$$\ddot{y} + gk_3\dot{y} + gk_4(y - y_d) = 0. \tag{56}$$

Define

$$y_1 = \theta + k_1(x - x_d) + k_2\dot{x}, \tag{57}$$

$$y_2 = \phi - k_3(y - y_d) - k_4\dot{y}, \tag{58}$$

and consider the y_1 and y_2 dynamics given by

$$\dot{y}_1 = \dot{\theta} + k_1\dot{x} + k_2\ddot{x} = \dot{\theta} + k_1\dot{x} + k_2g\theta, \tag{59}$$

$$\dot{y}_2 = \dot{\phi} - k_3\dot{y} - k_4\ddot{y} = \dot{\phi} - k_3\dot{y} + k_4g\phi. \tag{60}$$

Define the sliding variables (s_1, s_2)

$$s_1 = \dot{y}_1 + \alpha_1 y_1, \tag{61}$$

$$s_2 = \dot{y}_2 + \alpha_2 y_2, \tag{62}$$

where $\alpha_i > 0$, $i = 1,2$, which can be simplified as

$$s_1 = \dot{\theta} + (k_2g + \alpha_1)\theta + (k_1 + \alpha_1k_2)\dot{x} + \alpha_1k_1(x - x_d), \tag{63}$$

$$s_2 = \dot{\phi} + (k_4g + \alpha_2)\phi - (k_3 + \alpha_2k_4)\dot{y} - \alpha_2k_3(y - y_d). \tag{64}$$

The dynamics of sliding variables are found simply by taking time derivative of the sliding variables as

$$\dot{s}_1 = \ddot{\theta} + (k_2g + \alpha_1)\dot{\theta} + (k_1 + \alpha_1k_2)g\theta + \alpha_1k_1\dot{x}, \tag{65}$$

$$\dot{s}_2 = \ddot{\phi} + (k_4g + \alpha_2)\dot{\phi} + (k_3 + \alpha_2k_4)g\phi - \alpha_2k_3\dot{y}. \tag{66}$$

Substituting the expressions for $\ddot{\phi}$ and $\ddot{\theta}$ from (46) and (47), respectively, we obtain

$$\dot{s}_1 = f_2(\phi, \theta, \Psi) + u_3 + (k_2g + \alpha_1)\dot{\theta} + (k_1 + \alpha_1k_2)g\theta + \alpha_1k_1\dot{x}, \tag{67}$$

$$\dot{s}_2 = f_1(\phi, \theta, \Psi) + u_2 + (k_4g + \alpha_2)\dot{\phi} + (k_3 + \alpha_2k_4)g\phi - \alpha_2k_3\dot{y}. \tag{68}$$

We choose the inputs u_2 and u_3 as

$$u_2 = -\lambda_2 \operatorname{sign}(s_2) - f_1(\phi, \theta, \Psi) - (k_4 g + \alpha_2)\dot{\phi} - (k_3 + \alpha_2 k_4) g\phi + \alpha_2 k_3 \dot{y}, \tag{69}$$

$$u_3 = -\lambda_1 \operatorname{sign}(s_1) - f_2(\phi, \theta, \Psi) - (k_2 g + \alpha_1)\dot{\theta} - (k_1 + \alpha_1 k_2) g\theta - \alpha_1 k_1 \dot{x}, \tag{70}$$

so that the following closed-loop response for the sliding variables is obtained:

$$\dot{s}_1 = -\lambda_1 \operatorname{sign}(s_1), \tag{71}$$

$$\dot{s}_2 = -\lambda_2 \operatorname{sign}(s_2), \tag{72}$$

where we choose $\lambda_1 > 0$ and $\lambda_2 > 0$ large enough so that the terms F_d and τ_d are dominated by the sliding mode terms.

Now consider the Ψ-dynamics given by (48). The following control law stabilizes the Ψ-dynamics to $(\Psi, \dot{\Psi}) = (\Psi_d, 0)$:

$$u_4 = -k_5(\Psi - \Psi_d) - k_6 \dot{\psi} - f_3(\phi, \theta, \Psi), \tag{73}$$

where $k_5, k_6 > 0$.

The voltage inputs V_i, $i = 1, \ldots, 4$, are determined by substituting the expressions for the virtual control inputs u_i, $i = 1, \ldots, 4$, into Eqs. (34) and (42).

Consider Eqs. (31) and (35), and ignore F_d and τ_d. Then we have

$$\dot{v} = M^{-1} F_t - M^{-1} \hat{w} M v, \tag{74}$$

$$\dot{\omega} = \bar{J}^{-1} \tau_r - \bar{J}^{-1} (\dot{\bar{J}} + \hat{\omega} \bar{J}) \omega. \tag{75}$$

Eq. (30) can be rewritten as

$$\ddot{\eta} = \overline{m}^{-1} \left(-B_t^T \dot{v} - B_a^T \dot{w} + \tau_s - \dot{B}_t^T v - \dot{B}_a^T w - \dot{\overline{m}} \dot{\eta} + \frac{\partial L}{\partial \eta} \right), \tag{76}$$

which can be expressed in terms of F_t and τ_r as

$$\ddot{\eta} = \overline{m}^{-1} \left(\tau_s - \frac{B_t^T F_t}{m_t} - B_t^T \hat{\omega} v - B_a^T \bar{J}^{-1} (\tau_r - (\dot{\bar{J}} + \hat{\omega} \bar{J}) \omega) - \dot{B}_t^T v - \dot{B}_a^T w - \dot{\overline{m}} \dot{\eta} + \frac{\partial L}{\partial \eta} \right). \tag{77}$$

In order to have exponential convergence of the shape variables η to the desired η_d we choose τ_s as

$$\tau_s = \frac{B_t^T F_t}{m_t} + B_t^T \hat{\omega} v + B_a^T \bar{J}^{-1} (\tau_r - (\dot{\bar{J}} + \hat{\omega} \bar{J}) \omega) + \dot{B}_t^T v + \dot{B}_a^T w + \dot{\overline{m}} \dot{\eta} - \frac{\partial L}{\partial \eta} - \overline{m} \left(2\lambda \dot{\eta} + \lambda^2 (\eta - \eta_d) \right) \tag{78}$$

where $\lambda > 0$, so that

$$\ddot{\eta} + 2\lambda\dot{\eta} + \lambda^2(\eta - \eta_d) = 0. \tag{79}$$

4. Simulation

The controller developed in the previous sections is applied to the full nonlinear model of the aerial robot. The relevant parameter values of the system are listed in **Table 1**.

A rest-to-rest motion was simulated with initial conditions $(x_0, y_0, z_0) = (0, 0, 0)$, $(\phi_0, \theta_0, \Psi_0) = (0, 0, 0)$, and $(\theta_{10}, \theta_{20}) = (0, 0)$. The desired position, attitude, and joint angles were set as $(x_d, y_d, z_d) = (30, 50, 40)$ [m], $(\phi_d, \theta_d, \Psi_d) = (0, 0, 0)$, and $(\theta_{1d}, \theta_{2d}) = (30, 60)$ [°], respectively.

The control parameters are chosen as

$$(k_1, k_2, k_3, k_4, k_5, k_6) = (2, 0.1, 2, 0.1, 2, 2), \tag{80}$$

$$(\lambda_1, \lambda_2) = (1, 1), \ (\alpha_1, \alpha_2) = (0.1, 0.1). \tag{81}$$

As shown in **Figures 3–5**, the position, attitude, and joint angles converge to their desired values in around 40 s. **Figure 6** shows the time responses of the control inputs u_i, $i = 1,\ldots,4$.

Symbol	Parameter	Value	Unit
K_v	Transformation constant	54.945	rad s V^{-1}
J_r	Rotor inertia	6×10^{-5}	kg m^2
J_{xx}	MOI about x axis	0.0552	kg m^2
J_{yy}	MOI about y axis	0.0552	kg m^2
J_{zz}	MOI about z axis	0.1104	kg m^2
b	Thrust coefficient	3.935139×10^{-6}	N V^{-1}
d	Drag coefficient	1.192564×10^{-7}	Nm V^{-1}
l	Distance from pivot to motor	0.1969	m
m	Mass	2.85	kg
g	Acceleration of gravity	9.81	ms^{-2}
V	Maximum input voltage	10	V
m_1	Mass of link 1	0.1	kg
m_2	Mass of link 2	0.1	kg
m_p	Mass of the payload	0.1	kg
l_1	Length of link 1	0.5	m
l_2	Length of link 2	0.5	m

Table 1. Parameters of the aerial robot.

http://dx.doi.org/10.5772/intechopen.69641

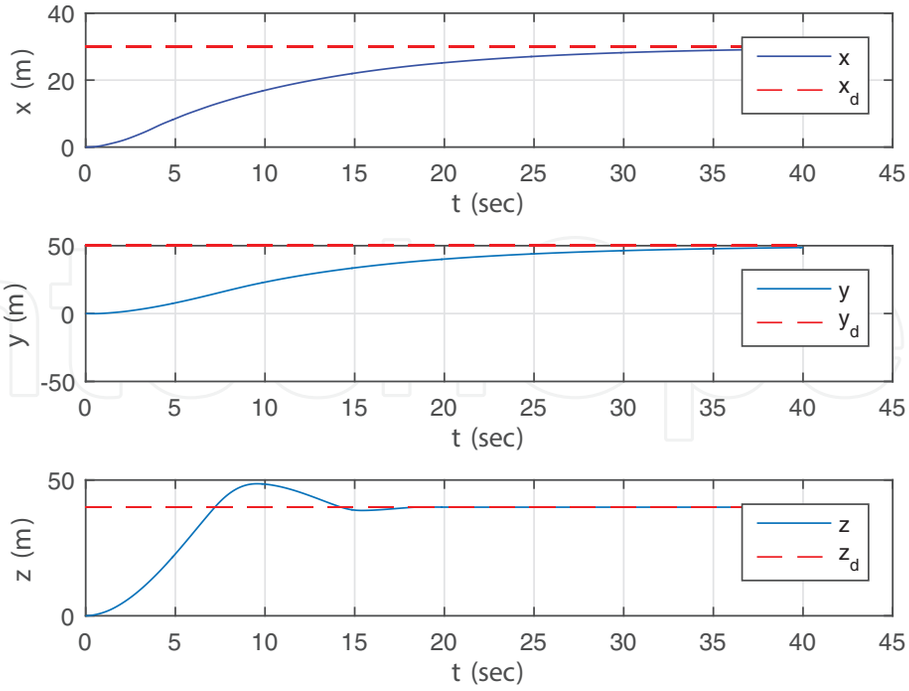

Figure 3. Time responses of the aerial robot's position x, y, and z.

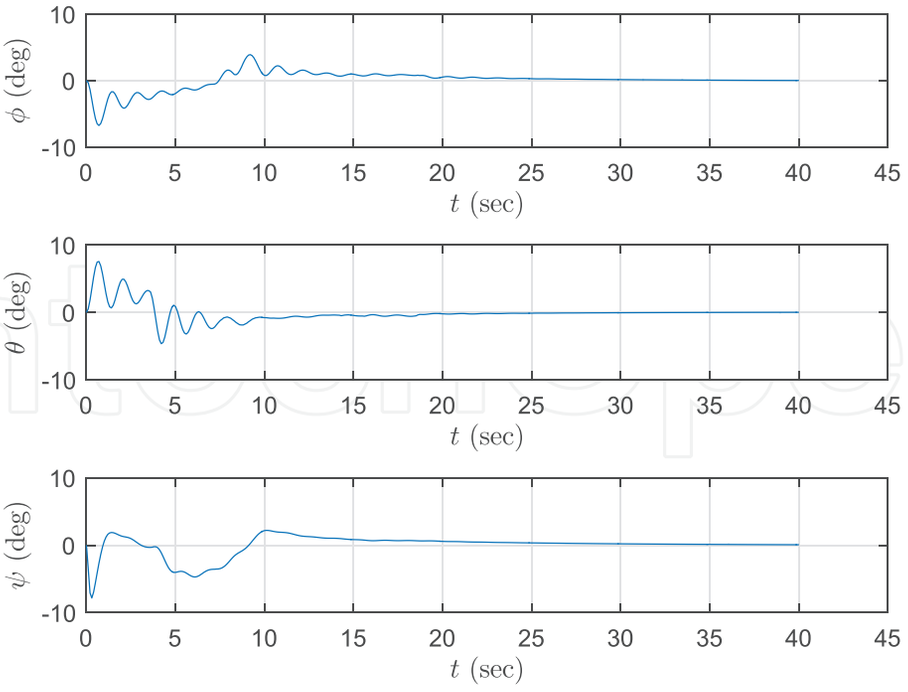

Figure 4. Time responses of the aerial robot's Euler angles ϕ, θ, and Ψ.

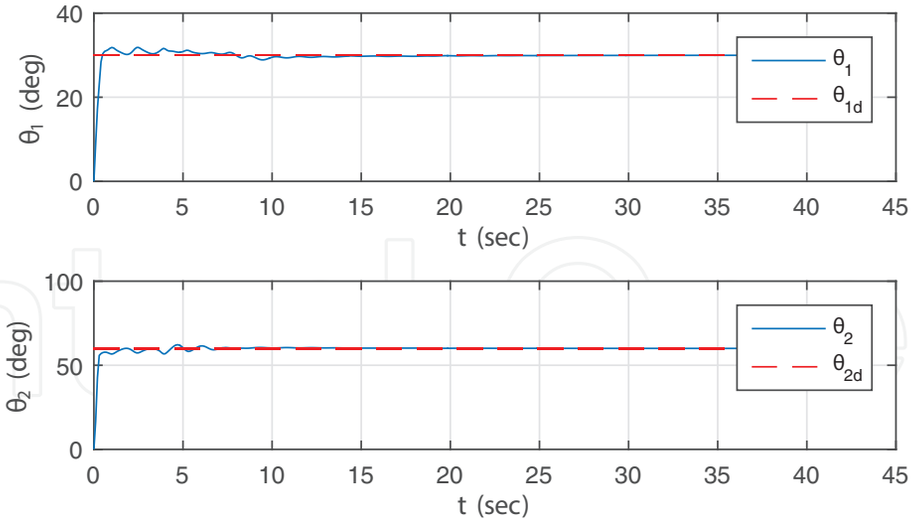

Figure 5. Time responses of the robotic arm's joint angles θ_1 and θ_2.

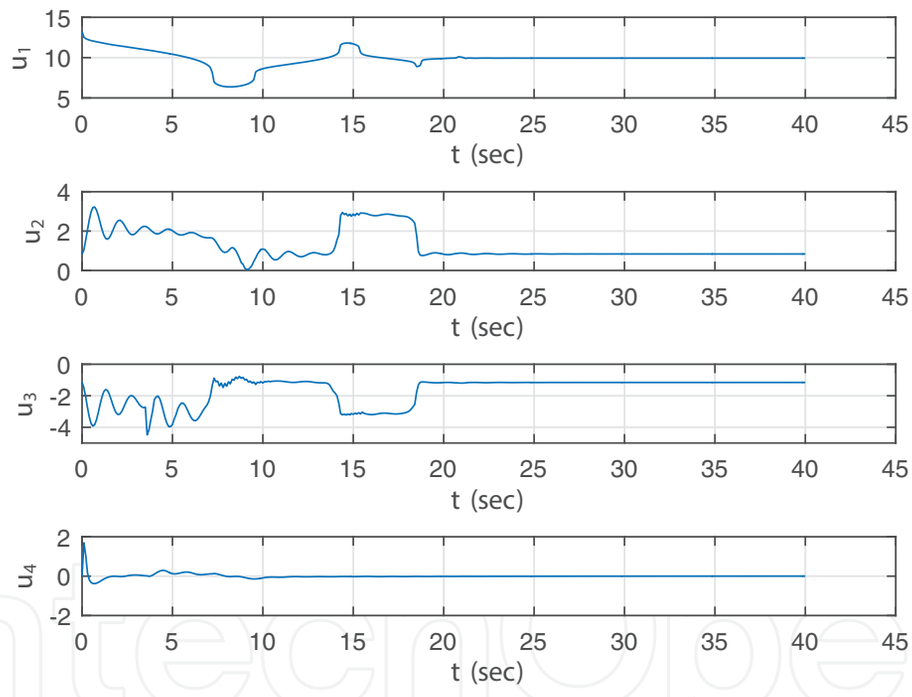

Figure 6. Time responses of the control inputs u_i, $i = 1,\ldots,4$.

5. Conclusions

This chapter first derives the complete nonlinear dynamics of an aerial robot consisting of a quadcopter with a two-link robot manipulator. Precise control of such an aerial robot is a challenging task since the translational and rotational dynamics of the quadcopter are strongly coupled with the dynamics of the manipulator. We extend our previous results on the control of quadrotor UAVs to the control of aerial robots. In particular, we design a backstepping and

Lyapunov-based nonlinear feedback control law that achieves the point-to-point control of the areal robot. The effectiveness of this feedback control law is illustrated through a simulation example.

The many avenues considered for future research include problems involving collaborative control of multiple aerial robots. Future research also includes designing nonlinear control laws that achieve robustness, insensitivity to system and control parameters, and improved disturbance rejection. We also plan to explore the use of geometric mechanics formulation of such control problems.

Appendix A

The matrices M and $\bar{J}$ can be expressed as

$$M = m_t \begin{bmatrix} 1 & 0 & 0 \\ 0 & 1 & 0 \\ 0 & 0 & 1 \end{bmatrix}, \; \bar{J} = \begin{bmatrix} \bar{J}_{11} & \bar{J}_{12} & \bar{J}_{13} \\ \bar{J}_{21} & \bar{J}_{22} & \bar{J}_{23} \\ \bar{J}_{31} & \bar{J}_{32} & \bar{J}_{33} \end{bmatrix},$$

where

$$\begin{aligned}
\bar{J}_{11} &= J_{xx} + [m_1 l_{c1}^2 + (m_2 + m_p) l_1^2 + \frac{1}{12} m_1 l_1^2] \sin^2\theta_1 + [m_2 l_{c2}^2 + m_p l_2^2 + \frac{1}{12} m_2 l_2^2] \sin^2\theta_2 \\
&\quad + 2 l_1 (m_2 l_{c2} + m_p l_2) \sin\theta_1 \sin\theta_2, \\
\bar{J}_{22} &= J_{yy} + m_1 l_{c1}^2 + (m_2 + m_p) l_1^2 + (m_2 l_{c2}^2 + m_p l_2^2) + 2 l_1 (m_2 l_{c2} + m_p l_2) \cos(\theta_2 - \theta_1) \\
&\quad + \frac{1}{12} [m_1 l_1^2 + m_2 l_2^2], \\
\bar{J}_{33} &= J_{zz} + [m_1 l_{c1}^2 + (m_2 + m_p) l_1^2 + \frac{1}{12} m_1 l_1^2] \cos^2\theta_1 + [m_2 l_{c2}^2 + m_p l_2^2 + \frac{1}{12} m_2 l_2^2] \cos^2\theta_2 \\
&\quad + 2 l_1 (m_2 l_{c2} + m_p l_2) \cos\theta_1 \cos\theta_2, \\
\bar{J}_{12} &= \bar{J}_{21} = \bar{J}_{23} = \bar{J}_{32} = 0, \\
\bar{J}_{13} &= \bar{J}_{31} = -\frac{1}{2} [m_1 l_{c1}^2 + (m_2 + m_p) l_1 + \frac{1}{12} m_1 l_1^2] \sin 2\theta_1 \\
&\quad - l_1 (m_2 l_{c2} + m_p l_2) \sin(\theta_1 + \theta_2) - \frac{1}{2} [(m_2 l_{c2}^2 + m_p l_2^2) + \frac{1}{12} m_2 l_2^2] \sin 2\theta_2.
\end{aligned}$$

The matrix $\overline{m}$ can be computed as

$$\overline{m} = \begin{bmatrix} m_1 l_{c1}^2 + (m_2 + m_p) l_1^2 + \frac{1}{12} m_1 l_1^2 & (m_2 l_{c2} + m_p l_2) l_1 \cos(\theta_2 - \theta_1) \\ (m_2 l_{c2} + m_p l_2) l_1 \cos(\theta_2 - \theta_1) & m_2 l_{c2}^2 + m_p l_2^2 + \frac{1}{12} m_2 l_2^2 \end{bmatrix}.$$

The matrices K, B_r, and B_t are given by

$$K = \begin{bmatrix} 0 & -K_{xy} & 0 \\ K_{xy} & 0 & -K_{xz} \\ 0 & K_{xz} & 0 \end{bmatrix}, \; B_r = \begin{bmatrix} 0 & 0 \\ B_{r1} & B_{r2} \\ 0 & 0 \end{bmatrix},$$

where

$$K_{xy} = [m_1 l_{c1} + (m_2 + m_p) l_1] \sin\theta_1 + (m_2 l_{c2} + m_p l_2) \sin\theta_2,$$
$$K_{xz} = [m_1 l_{c1} + (m_2 + m_p) l_1] \cos\theta_1 + (m_2 l_{c2} + m_p l_2) \cos\theta_2,$$
$$B_{r1} = -[m_1 l_{c1}^2 + (m_2 + m_p) l_1^2 + (m_2 l_{c2} + m_p l_2) l_1 \cos(\theta_2 - \theta_1)] + \frac{1}{12} m_1 l_1^2,$$
$$B_{r2} = -[m_2 l_{c2}^2 + m_p l_2^2 + (m_2 l_{c2} + m_p l_2) l_1 \cos(\theta_2 - \theta_1)] + \frac{1}{12} m_2 l_2^2,$$

and

$$B_t = \begin{bmatrix} -(m_1 l_{c1} + m_2 l_1 + m_p l_1) \sin\theta_1 & -(m_2 l_{c2} + m_p l_2) \sin\theta_2 \\ 0 & 0 \\ (m_1 l_{c1} + m_2 l_1 + m_p l_1) \cos\theta_1 & (m_2 l_{c2} + m_p l_2) \cos\theta_2 \end{bmatrix}.$$

Author details

Mahmut Reyhanoglu* and Muhammad Rehan

*Address all correspondence to: mreyhanoglu@icloud.com

University of North Carolina Asheville, One University Heights, Asheville, NC, USA

References

[1] Brezoescu A, Espinoza T, Castillo P, Lozano R. Adaptive trajectory following for a fixed-wing UAV in presence of crosswind. Journal of Intelligent and Robotic Systems. 2013;69:257–271

[2] Espinoza T, Dzul A, Llama M. Linear and nonlinear controllers applied to fixed-wing UAV. International Journal of Advanced Robotics Systems. 2006;10:1–10

[3] Ferreira HC, Baptista RS, Ishihara JY, Borges GA. Disturbance rejection in a fixed wing UAV using nonlinear H_∞ state feedback. In: Proceedings of International Conference on Control and Automation. 2011. pp. 386–391

[4] Gavilan F, Acosta JA, Vazquez R. Control of the longitudinal flight dynamics of an UAV using adaptive backstepping. In: Proceedings of the 18th IFAC World Congress. 2011. pp. 1892–1897

[5] Hervas JR, Kayacan E, Reyhanoglu M, Tang H. Sliding mode control of fixed-wing UAVs in the presence of stochastic wind. In: Proceedings of International Conference on Control, Automation, Robotics and Vision. 2014. pp. 986–991

[6] Hervas JR, Reyhanoglu M, Tang H. Automatic landing control of unmanned aerial vehicles on moving platforms. In: Proceedings of IEEE International Symposium on Industrial Electronics. 2014. pp. 69–74

[7] Hervas JR, Reyhanoglu M, Tang H. Nonlinear automatic landing control of unmanned aerial vehicles on moving platforms via a 3D laser radar. In: AIP Proceedings. 2014. pp. 907–917

[8] Hervas JR, Reyhanoglu M, Tang H, Kayacan E. Nonlinear control of fixed-wing UAVs in presence of stochastic winds. Communications in Nonlinear Science and Numerical Simulation. 2016;33:57–69

[9] Kannan S, Alma M, Olivares-Mendez MA, Voos H. Adaptive control of aerial manipulation vehicle. In: Proceedings of IEEE International Conference on Control System, Computing and Engineering. 2014. pp. 1–6

[10] Kayacan E, Khanesar MA, Hervas JR, Reyhanoglu M. Intelligent control of unmanned aerial vehicles using fuzzy neural networks. International Journal of Aerospace Engineering. 2017:2017:1–13

[11] Liu C, McAree O, Chen WH. Path-following control for small fixed-wing unmanned aerial vehicles under wind disturbances. International Journal of Robust and Nonlinear Control. 2013;23:1682–1698

[12] MacKunis W, Wilcox ZD, Kaiser MK, Dixon WE. Global adaptive output feedback tracking control of an unmanned aerial vehicle. IEEE Transactions on Control Systems Technology. 2010;18:1390–1397

[13] Chen X, Wang L. Cascaded model predictive control of a quadrotor UAV. In: Proceedings of Australian Control Conference. 2013. pp. 354–359

[14] Huang H, Hoffmann GM, Waslander SL, Tomlin CJ. Aerodynamics and control of autonomous quadrotor helicopters in aggressive maneuvering. In: Proceedings of International Conference on Robotics and Automation. 2009. pp. 3277–3282

[15] Shulong Z, Honglei A, Daibing Z, Lincheng S. A new feedback linearization LQR control for attitude of quadrotor. In: Proceedings of International Conference on Control, Automation, Robotics and Vision. 2013. pp. 1593–1597

[16] Damen R, Reyhanoglu M, MacKunis W, Hervas JR. Passivity-based quaternion feedback control of a hover system. In: Proceedings of International Conference on Control, Automation and Systems. 2016. pp. 201–206

[17] Reyhanoglu M, Damen R, MacKunis W. Observer-based sliding mode control of a 3-DOF hover system. In: Proceedings of International Conference on Control, Automation, Robotics and Vision. 2016. pp. 1–6

[18] Stebler S, Campobasso M, Kidambi K, MacKunis W, Reyhanoglu M. Dynamic neural network-based sliding mode estimation of quadrotor systems. In: Proceedings of American Control Conference. 2017. pp. 1–6

[19] Stebler S, MacKunis W, Reyhanoglu M. Nonlinear output feedback tracking control of a quadrotor UAV in the presence of uncertainty. In: Proceedings of International Conference on Control, Automation, Robotics and Vision. 2016. pp. 1–6

[20] Alvarez-Munoz JU, Marchand N, Guerrero-Castellanos F, Durand S, Lopez-Luna AE. Improving control of quadrotors carrying a manipulator arm. In: Proceedings of XVI Congreso Latinoamericano de Control Automatico. 2014. pp. 1–6

[21] Arleo G, Caccavale F, Muscio G, Pierri F. Control of quadrotor aerial vehicles equipped with a robotic arm. In: Proceedings of Mediterranean Conference on Control & Automation. 2013. pp. 1–7

[22] Heredia G, Jimenez-Cano AE, Sanchez I, Llorente D, Vega V, Braga J, Acosta JA, Ollero A. Control of a multirotor outdoor aerial manipulator. In: Proceedings of IEEE/RSJ International Conference on Intelligent Robots and Systems. 2014. pp. 3417–3422

[23] Kang Y, Hedrick JK. Linear tracking for a fixed-wing UAV using nonlinear model predictive control. IEEE Transactions on Control Systems Technology. 2009;17:1202–1210

[24] Kobilarov M. Nonlinear trajectory control of multi-body aerial manipulators. Journal of Intelligent Robotic Systems. 2014;73:679–692

[25] Lee D, Nataraj C, Burg TC, Dawson DM. Adaptive tracking control of an underactuated aerial vehicle. In: Proceedings of American Control Conference. 2011. pp. 2326–2331

[26] Lee D, Burg TC, Dawson DM, Shu D, Xian B, Tatlicioglu E. Robust tracking control of an underactuated quadrotor aerial-robot based on a parametric uncertain model. In: Proceedings of IEEE International Conference on Systems, Man and Cybernetics. 2009. pp. 3187–3192

[27] Orsag M, Korpela C, Pekala M, Oh P. Stability control in aerial manipulation. In: Proceedings of American Control Conference. 2013. pp. 5581–5586

[28] Cho S, McClamroch NH, Reyhanoglu M. Dynamics of multibody vehicles and their formulation as nonlinear control systems. In: Proceedings of American Control Conference. 2000. pp. 3908–3912

[29] Meirovitch L, Kwak MK. State equations for a spacecraft with maneuvering flexible appendages in terms of quasi-coordinates. Applied Mechanics Reviews. 1989;42:161–170

[30] Reyhanoglu M, van der Schaft AJ, McClamroch NH, Kolmanovsky I. Nonlinear control of a class of underactuated systems. Proceedings of IEEE Conference on Decision and Control. 1996. pp. 1682–1687

[31] Reyhanoglu M, van der Schaft AJ, McClamroch NH, Kolmanovsky I. Dynamics and control of a class of underactuated mechanical systems. IEEE Transactions on Automatic Control. 1999;44:1663–1671

[32] Reyhanoglu M, Cho S, McClamroch NH. Discontinuous feedback control of a special class of underactuated mechanical systems. International Journal of Robust and Nonlinear Control. 2000;10:265–281

[33] Reyhanoglu M. Maneuvering control problems for a spacecraft with unactuated fuel slosh dynamics. In: Proceedings of IEEE Conference on Control Applications. 2003. pp. 1–6

[34] Haimo VT. Finite time controllers. SIAM Journal on Control and Optimization. 1986;24: 760–770

IntechOpen